Energy & Environmental Science

COMMUNICATION

Cite this: DOI: 10.1039/c5ee02477c

Received 12th August 2015,
Accepted 5th October 2015

DOI: 10.1039/c5ee02477c

www.rsc.org/ees

A planar electron acceptor for efficient polymer solar cells†

Yao Wu,‡[a] Huitao Bai,‡[b] Zaiyu Wang,[c] Pei Cheng,[bd] Siya Zhu,[a] Yifan Wang,[bd] Wei Ma[c] and Xiaowei Zhan*[a]

A novel planar acceptor IDT-2BR was designed and synthesized. Polymer solar cells (PSCs) based on P3HT:IDT-2BR blended films gave power conversion efficiencies of up to 5.12%, which are much higher than that of $PC_{61}BM$-based control devices (3.71%) and the highest values reported for P3HT-based fullerene-free PSCs.

In the last 20 years, fullerene based electron acceptors have played an irreplaceable role in advancing the development of bulk heterojunction (BHJ) organic solar cells (OSCs).[1–6] Power conversion efficiencies (PCEs) of polymer solar cells (PSCs) utilizing [6,6]-phenyl-C_{61}-butyric acid methyl ester ($PC_{61}BM$) or [6,6]-phenyl-C_{71}-butyric acid methyl ester ($PC_{71}BM$) as electron acceptors increased from 2.5% to exceeding 10%.[7–10] As dominating electron acceptors for OSCs, fullerene derivatives show excellent characteristics, such as high electron affinity, high electron mobility, isotropic electron transporting ability, and the capability to form favorable nanoscale morphologies when mixed with electron donors.[11–13] However, they have also been suffering from some intrinsic drawbacks, such as poor photostability in air, morphological instability in thin film blends over time, poor solar energy harvesting in the visible region, restricted electronic tuning and purification problems.[14–16] Thus, recent studies have attempted to solve these problems of fullerene-based OSCs by developing new nonfullerene electron acceptor materials that possess strong, broad absorption and have appropriate energy levels, aiming to fabricate so-called fullerene-free OSCs.[17–21] Obviously, developing novel nonfullerene acceptors will enrich the number of known acceptor families, and provide more opportunities for the selection of donor/acceptor (D/A) pairs to obtain better PCEs. So far, a variety of novel nonfullerene acceptors with various electron-withdrawing groups have been exploited, and PCEs of exceeding 6% have been achieved.[22–42]

Broader context

Although fullerene derivatives have been dominant electron acceptors for solution-processed polymer solar cells (PSCs), they have been suffering from weak absorption in the visible spectral region, limited energy level variability, and easy diffusion and aggregation, leading to instability of morphology in the blended films. Thus, to enhance the performance of PSCs, development of new nonfullerene electron acceptor materials is necessary. Compared with low-bandgap polymers, regioregular poly(3-hexylthiophene) (P3HT) is easily synthesized by low cost methods, and still is the best choice for the production of large-area devices since it possesses a relatively stable nature under ambient conditions. However, P3HT-based fullerene-free PSCs exhibited relatively low power conversion efficiencies (PCEs) (the best PCEs were around 4.1%). In this work, we designed, calculated and synthesized a planar electron acceptor IDT-2BR with an A–D–A structure, using an indacenodithiophene (IDT) unit as a core and 5-(benzo[*c*][1,2,5]thiadiazol-4-ylmethylene)-3-ethyl-2-thioxothiazo-lidin-4-one (BR) units as end-capping electron-withdrawing groups. Theoretical calculations revealed that IDT-2BR adopted a nearly flat backbone configuration while the hexylphenyl groups on the IDT moiety exhibited a dihedral angle of *ca.* 115° to the backbone plane. IDT-2BR exhibited excellent thermal stability, broad and strong absorption from 300 to 750 nm with a maximum extinction coefficient of 1.3×10^5 M^{-1} cm^{-1} at 636 nm, appropriate LUMO (−3.69 eV) and HOMO (−5.52 eV) energy levels matched with those of P3HT, and a relatively high electron mobility of 3.4×10^{-4} cm^2 V^{-1} s^{-1}. Fullerene-free PSCs based on P3HT:IDT-2BR blended films gave PCEs of up to 5.12%, which is much higher than that of $PC_{61}BM$-based control devices (3.71%) and is the highest value reported for P3HT-based fullerene-free PSCs. Interestingly, the PCE values changed only 10% when varying the thickness of the active layer from 60 nm to 220 nm, which is beneficial to device reproducibility and scalable roll-to-roll fabrication.

[a] *Department of Materials Science and Engineering, College of Engineering, Key Laboratory of Polymer Chemistry and Physics of Ministry of Education, Peking University, Beijing, 100871, P. R. China. E-mail: xwzhan@pku.edu.cn*
[b] *Beijing National Laboratory for Molecular Sciences, Key Laboratory of Organic Solids, Institute of Chemistry, Chinese Academy of Sciences, Beijing, 100190, P. R. China*
[c] *State Key Laboratory for Mechanical Behavior of Materials, Xi'an Jiaotong University, Xi'an, 710049, P. R. China*
[d] *University of Chinese Academy of Sciences, Beijing, 100049, P. R. China*

† Electronic supplementary information (ESI) available: Experimental details, density functional theory calculation details, TGA curves of IDT-2BR, *J–V* curves of the devices based on P3HT:IDT-2BR with different donor/acceptor ratios, data of the OSCs based on P3HT : IDT-2BR blends (1 : 0.6, w/w) with 3% CN with various active layer thicknesses, *J–V* and IPCE curves of the device based on P3HT : $PC_{61}BM$ (1 : 1, w/w), SCLC device characteristics of IDT-2BR and P3HT : IDT-2BR (1 : 0.6, w/w) blended films and two-dimensional GIWAXS patterns of P3HT, IDT-2BR and P3HT : IDT-2BR (1 : 0.6, w/w) blended films. See DOI: 10.1039/c5ee02477c

‡ Yao Wu and Huitao Bai contributed equally.

Recently, we developed a series of acceptor–donor–acceptor (A–D–A) type small molecule acceptors utilizing indacenodithiophene (IDT) or indacenodithienothiophene units as the core and different electron-withdrawing units as end-capping groups.[37–39,43,44] Compared with the previously reported molecular structures of perylene diimide (PDI) dimers or trimers, the design of the A–D–A structure provides an effective way to tune energy levels by introducing end-capping groups with different electron-withdrawing abilities. Moreover, the extended conjugation of the IDT units facilitates π-electron delocalization, reduces the bandgap and broadens absorption. The rigid and coplanar structure of IDT can prevent the molecular skeleton from torsional or conformational changes, and enhance charge carrier mobility.[45,46] Finally, the tetrahexylphenyl groups as peripheral substituents of the coplanar backbone ensure solution processability, reduce intermolecular interactions, and prevent the acceptor from strong self-aggregation and large phase separation in blended films.

To maximize the performance of fullerene-free PSCs, more efficient low-bandgap polymers are selected as donor materials in the literature. However, the high-performance polymers for lab scale fabrication (a few mm^2) are limited in commercial large-area application due to their high cost and unstable nature in air.[47] As the most representative and thoroughly studied polymer donor material, regioregular poly(3-hexylthiophene) (P3HT) is easily synthesized by low cost methods. Compared with other low-bandgap polymers, P3HT is still the best choice for the production of large-area devices since it possesses a relatively stable nature under ambient conditions, and the photovoltaic performance of P3HT-based PSCs is insensitive to the thickness of the active layers.[48] However, P3HT-based fullerene-free PSCs exhibited relatively low PCEs (the best PCEs were around 4.1%).[43,49–60] Recently, McCulloch and coworkers reported a small molecule non-fullerene acceptor FBR bearing the 5-(benzo-[*c*][1,2,5]thiadiazol-4-ylmethylene)-3-ethyl-2-thioxothiazolidin-4-one (BR) unit. Inverted PSCs employing P3HT as the donor and FBR as the acceptor gave high PCEs of up to 4.1%.[57]

In this work, we developed a planar electron acceptor IDT-2BR (Scheme 1) using an IDT unit as a core and a BR unit as an end-capping group. Compound IDT-2BR exhibited strong and broad absorption, appropriate energy levels matching with those of P3HT, relatively high electron mobility, and suitable phase separation when blended with P3HT. Solution-processed BHJ PSCs based on P3HT:IDT-2BR achieved PCEs as high as 5.12%, which is much higher than that of $PC_{61}BM$-based control devices (3.71%) and is the highest value reported for P3HT-based fullerene-free PSCs. The PCE values changed only 10% when varying the thickness of the active layer from 60 nm to 220 nm.

Density functional theory calculations were carried out to investigate the molecular geometries and molecular frontier orbitals of IDT-2BR using the Gaussian 09 program (Fig. 1). The computation details are described in the ESI.† As shown in Fig. 1, the molecule adopts a nearly flat backbone configuration while the hexylphenyl groups on the IDT moiety exhibit a dihedral angle of *ca.* 115° to the backbone plane. The coplanar backbone structure is beneficial to π–π stacking which offers an advantage of obtaining high charge carrier mobility, and the

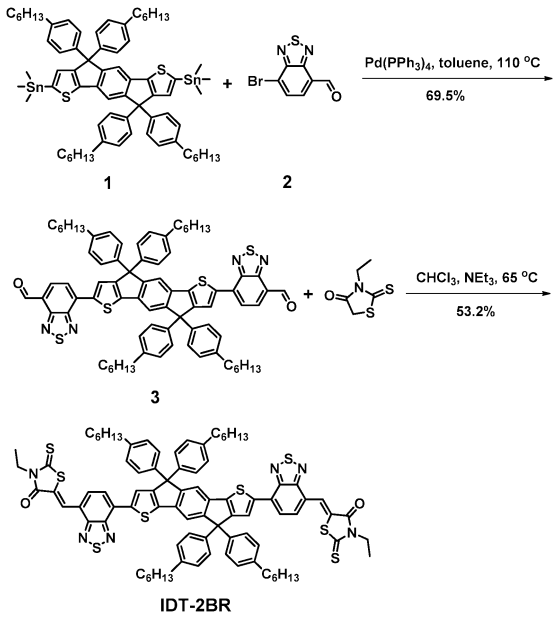

Scheme 1 The synthetic route of IDT-2BR.

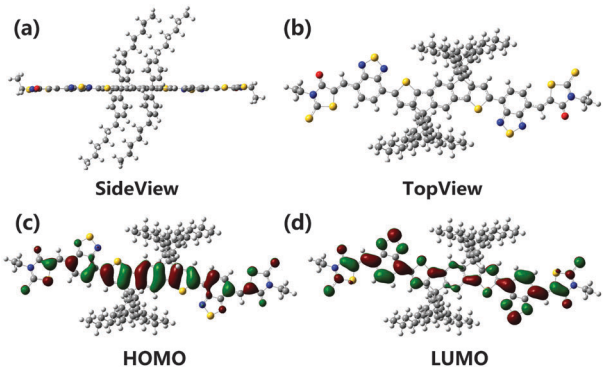

Fig. 1 (a and b) Optimized geometries and (c and d) molecular orbitals of IDT-2BR.

steric effect of tetrahexylphenyl substituents helps to reduce intermolecular interactions and restrict the severe self-aggregation and large-scale phase separation in the blended films. The HOMO orbital of IDT-2BR is distributed on the IDT, benzothiadiazole (BT) and the linked double bond, while the LUMO orbital is delocalized across the entire backbone, which is beneficial to electron transport.

The synthetic route to IDT-2BR is depicted in Scheme 1. Compound IDT-2BR was synthesized *via* two facile reactions. The new intermediate **3** was synthesized in 69.5% yield through Stille coupling reaction between two commercially available reagents **1** and **2** using $Pd(PPh_3)_4$ as the catalyst. Subsequent Knoevenagel condensation between compound **3** and 3-ethyl-rhodanine afforded IDT-2BR in 53.2% yield. Compounds **3** and IDT-2BR were fully characterized by matrix-assisted laser desorption/ionization-time-of flight mass spectrometry (MALDI-TOF MS), ^{1}H-NMR, ^{13}C-NMR, and elemental analysis. IDT-2BR is readily soluble in common organic solvents, such as dichloromethane (DCM), chloroform (CF) and *o*-dichlorobenzene (*o*-DCB) at room

temperature (>15 mg mL^{-1}). The thermal properties of IDT-2BR were investigated by thermogravimetric analysis (TGA). The compound exhibits excellent thermal stability with a decomposition temperature (5% weight loss) at 367 °C in a nitrogen atmosphere (Fig. S1, ESI†).

The normalized spectra of optical absorption of IDT-2BR in chloroform solution (10^{-6} M) and in solid film are shown in Fig. 2a. The IDT-2BR solution exhibits broad and strong absorption in the 300–750 nm region with a maximum extinction coefficient of 1.3×10^5 M^{-1} cm^{-1} at 636 nm. Compared with the solution, the IDT-2BR film shows a red-shifted peak of 658 nm with a resolved shoulder, indicating that self-organization behaviour does exist in the film. Since the absorption of the P3HT film mainly is located in the range of 400–600 nm, the complementary absorption of IDT-2BR and P3HT is beneficial to harvesting light in the visible region when using IDT-2BR as an acceptor to blend with P3HT. The optical bandgap estimated from the absorption edge (736 nm) of the thin film is 1.68 eV.

The electrochemical properties of IDT-2BR were studied by cyclic voltammetry (CV) with the IDT-2BR film on a glassy carbon working electrode in 0.1 M $[^nBu_4N]^+[PF_6]^-$ CH_3CN solution at a potential scan rate of 100 mV s^{-1}. As shown in Fig. 2b, IDT-2BR exhibits reversible reduction and quasi-reversible oxidation waves. The onset oxidation and reduction potentials of IDT-2BR are 0.72 V and -1.11 V *versus* $FeCp_2^{0/+}$, respectively. Assuming the absolute energy level of $FeCp_2^{0/+}$ to be 4.8 eV below vacuum, the HOMO and LUMO levels are estimated to be -5.52 eV and -3.69 eV from onset oxidation and reduction potentials, respectively. The LUMO level of IDT-2BR is higher than that of $PC_{61}BM$ (-3.9 eV),[11] and an improved open circuit voltage (V_{OC}) relative to $PC_{61}BM$ is expected. The HOMO and LUMO energy levels match with those of wide-bandgap polymer donors such as P3HT.

The electron acceptor performance of IDT-2BR was investigated in BHJ PSCs with a configuration of ITO/PEDOT:PSS/P3HT:IDT-2BR/Ca/Al using P3HT as the electron donor material. Fig. S2 (ESI†) and Fig. 3a show the *J*–*V* curves of the devices, and Table 1 lists the detailed device parameters including V_{OC}, short circuit current density (J_{SC}), fill factor (FF), and PCE at different D/A weight ratios. These devices yielded higher V_{OC} (0.83–0.85 V) than that of $PC_{61}BM$-based control devices (0.61 V) due to the higher LUMO level of IDT-2BR. The blend at a D/A weight ratio of 1 : 0.6 gave the best performance: the V_{OC}, J_{SC}, FF, and PCE are 0.85 V, 6.38 mA cm^{-2}, 69.0% and 3.72%, respectively. To improve the morphologies and photovoltaic performance of the blended films, 1-chloronaphthalene (CN) is adopted as an additive in the solution. Addition of 1–5% (v/v) CN improves the J_{SC} value from 6.38 to 7.53–8.91 mA cm^{-2} with little change in V_{OC} and FF. PSC devices with 3% CN show significantly improved performance: the V_{OC}, J_{SC}, FF, and PCE reaches 0.84 V, 8.91 mA cm^{-2}, 68.1%, and 5.12%, respectively. To our knowledge, the FF of 68.1% and the PCE of 5.12% are the highest values reported for P3HT-based fullerene-free solar cells. To compare the acceptor performance of IDT-2BR and $PC_{61}BM$, PSC devices based on the P3HT : $PC_{61}BM$ (1 : 1, w/w) blend were

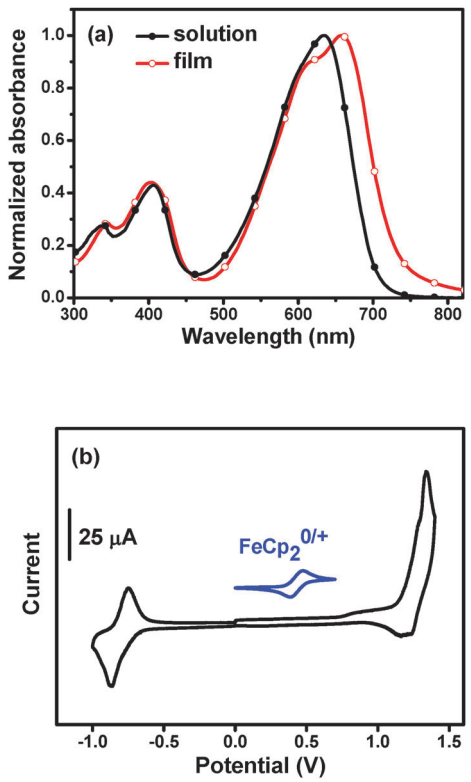

Fig. 2 (a) Absorption spectra of IDT-2BR in chloroform solution and film; (b) cyclic voltammogram for IDT-2BR in CH_3CN/0.1 M Bu_4NPF_6 at 100 mV s^{-1}; the horizontal scale refers to an Ag/AgCl electrode as a reference electrode.

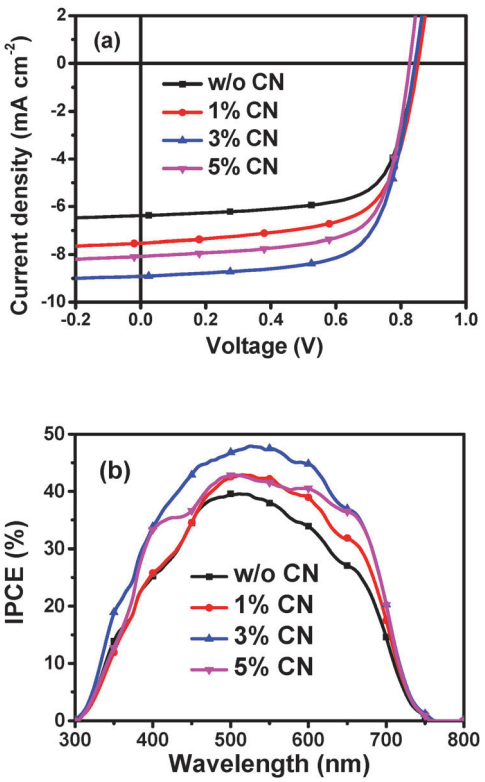

Fig. 3 (a) The *J*–*V* curves of the devices based on P3HT : IDT-2BR (1 : 0.6, w/w) processed with different CN concentrations under the illumination of AM 1.5G, 100 mW cm^{-2}; (b) IPCE curves of corresponding devices.

Table 1 Photovoltaic performances of the OSCs based on P3HT:IDT-2BR blends under the illumination of AM 1.5G, 100 mW cm^{-2}

Acceptor	D/A ratio (w/w)	CN (%)	V_{OC} (V)	J_{SC} (mA cm^{-2})	FF (%)	PCE (%) Best	PCE (%) Ave.[b]
IDT-2BR	1 : 1	—	0.84	5.99	69.4	3.49	3.31
	1 : 0.8	—	0.84	6.07	70.2	3.58	3.38
	1 : 0.6	—	0.85	6.38	69.0	3.72	3.56
		1	0.85	7.53	65.9	4.23	4.13
		3	0.84	8.91	68.1	5.12	5.04
		5	0.83	8.08	69.6	4.65	4.51
	1 : 0.5	—	0.85	6.56	60.2	3.34	3.22
$PC_{61}BM$[a]	1 : 1	—	0.61	8.66	69.9	3.71	3.63

[a] Thermal annealing at 140 °C for 10 min. [b] The average PCE is obtained from over 30 devices.

also fabricated, which gave a lower V_{OC} of 0.61 V, a similar J_{SC} of 8.66 mA cm^{-2}, a similar FF of 69.9%, and a lower PCE of 3.71% after thermal annealing at 140 °C for 10 min (Fig. S3a, ESI†). In contrast to the $PC_{61}BM$ counterpart, IDT-2BR-based devices yielded higher V_{OC} without reducing J_{SC} and FF.

Fig. 3b shows the incident photons to converted current efficiency (IPCE) curves of the devices based on P3HT : IDT-2BR (1 : 0.6, w/w) processed with different CN concentrations. The IPCE curves of these devices cover a broad response of 300–750 nm. The IPCE in 300–650 nm is attributed to P3HT absorption (Fig. S3b, ESI†), while that in 650–750 nm is attributed to IDT-2BR absorption. The J_{SC} calculated from integration of the IPCE spectra with the AM 1.5G reference spectrum is 6.35, 7.30, 8.51, and 7.85 mA cm^{-2} with addition of 0%, 1%, 3%, 5% CN, respectively, which is similar to that obtained from *J–V* measurement (the average error is 5%).

Interestingly, the PCE values changed only 10% when varying the thickness of the active layer from 60 nm to 220 nm (Fig. 4, Table S1, ESI†). This feature is very important to device reproducibility and scalable roll-to-roll fabrication.

The bimolecular recombination in the devices based on P3HT : IDT-2BR (1 : 0.6, w/w) was assessed by measuring the dependence of J_{SC} on light intensity. The correlation between J_{SC} and illumination intensity (P) was expressed by $J_{SC} \propto P^{\alpha}$, where an α value close to 1 indicates weak bimolecular

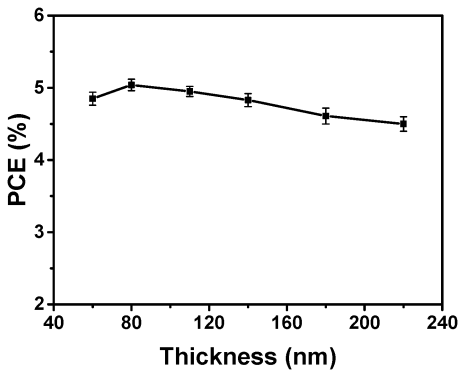

Fig. 4 PCEs of the OSCs based on P3HT : IDT-2BR blends (1 : 0.6, w/w) with 3% CN with various active layer thicknesses.

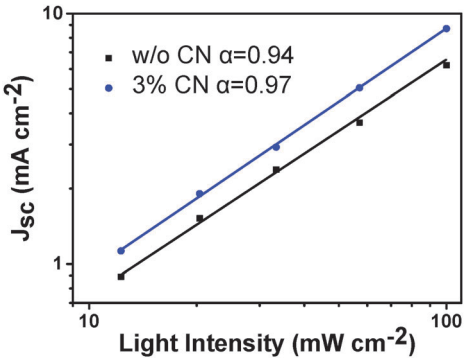

Fig. 5 Dependence of J_{SC} on light intensity for the devices based on P3HT : IDT-2BR (1 : 0.6, w/w) processed without CN and with 3% (v/v) CN.

recombination in the OSC devices.[61,62] As shown in Fig. 5, the α value of the devices based on P3HT : IDT-2BR (1 : 0.6, w/w) processed without CN and with 3% (v/v) CN were 0.94 and 0.97, respectively. The higher α value which is closer to 1 suggests weaker bimolecular recombination existing in the device processed with 3% CN. The decreased bimolecular recombination is beneficial to higher J_{SC} and better device performance.

To understand the influence of charge carrier transport on photovoltaic performance, the electron mobility of the IDT-2BR pristine film and the electron and hole mobilities of P3HT : IDT-2BR (1 : 0.6, w/w) blended films were measured by the space-charge limited current (SCLC) method with the device structure: ITO/PEDOT:PSS/active layer/Au for holes and Al/active layer/Al for electrons (Fig. S4, ESI†), and the data are summarized in Table S2 in the ESI.† IDT-2BR pristine film exhibits a relatively high electron mobility of 3.4×10^{-4} cm^2 V^{-1} s^{-1}. The blended film of P3HT : IDT-2BR (1 : 0.6, w/w) without CN exhibits a hole mobility of 6.1×10^{-4} cm^2 V^{-1} s^{-1} and an electron mobility of 1.5×10^{-4} cm^2 V^{-1} s^{-1}. After addition of 3% CN, the blended film exhibits a decreased hole mobility of 2×10^{-4} cm^2 V^{-1} s^{-1} and an enhanced electron mobility of 2.6×10^{-4} cm^2 V^{-1} s^{-1} with better hole and electron transport balance, which is responsible for the higher FF and J_{SC} values. The $PC_{61}BM$-based control device exhibits a slightly higher electron mobility of 3.8×10^{-4} cm^2 V^{-1} s^{-1} but a lower hole mobility of 1.4×10^{-5} cm^2 V^{-1} s^{-1}.

The molecular orientation and packing of pure IDT-2BR, pure P3HT, P3HT:IDT-2BR blends without and with 3% CN was investigated by grazing incident wide angle X-ray scattering (GIWAXS). Fig. 6 shows GIWAXS profiles of IDT-2BR, P3HT and blend films with different processing conditions, and corresponding two-dimensional patterns are shown in Fig. S5 (ESI†). IDT-2BR shows an amorphous nature with no obvious diffraction peaks observed. The annealed pure P3HT exhibits a highly ordered structure, with strong (100), (200) and (300) peaks. The high crystallinity of P3HT is preserved after blending with IDT-2BR. It is well known that the π–π stacking is crucial for charge transport and thus the π–π stacking coherence length in the in-plane direction is calculated to be 7.9, 5.7 and 6.9 nm for the pure P3HT, blend without CN and with 3% CN, respectively. The out-of-plane (100) coherence length is 15.6 and 22.3 nm for the blend without CN and with 3% CN, respectively. The enhanced π–π

View Article Online
DOI: 10.1039/C5EE02477C

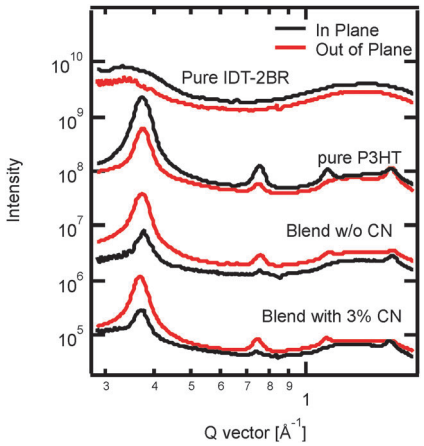

Fig. 6 GIWAXS profiles of IDT-2BR, P3HT pristine and blend (P3HT : IDT-2BR = 1 : 0.6, w/w) films without CN or with 3% CN on SiO_2/Si substrate. The curves are offset for clarity.

stacking in the in-plane direction and lamella stacking in the out-of-plane direction are achieved after processing with 3% CN. This phenomenon partially explains the better device performance obtained with 3% CN.

Tapping-mode atomic force microscopy (AFM) was used to investigate the surface morphology of the active layer. According to the AFM images (Fig. 7a and b), the blended film without CN exhibits a uniform but relatively rough surface with a root mean square (RMS) roughness of 12.4 nm. The blended film with 3% CN exhibits a rougher surface with a RMS roughness of 15.7 nm. Transmission electron microscopy (TEM) was used to investigate the internal morphology of the active layer (Fig. 7c and d). Addition of CN leads to clearer aggregation domains and interpenetrating networks, due to the enhanced crystallinity of P3HT, which is consistent with the GIWAXS results.

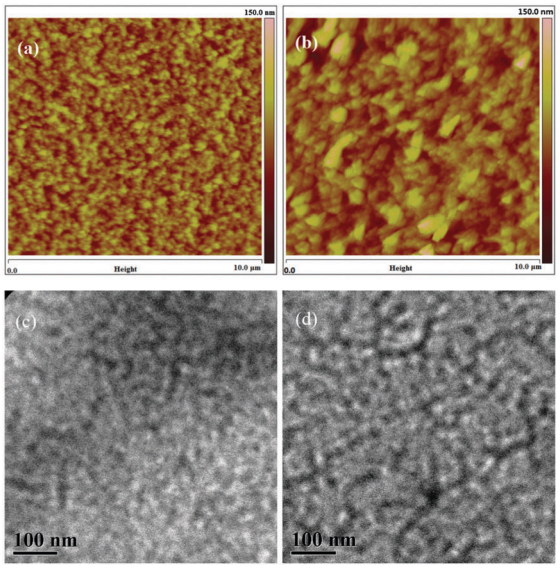

Fig. 7 AFM height (a and b) and TEM images (c and d) of P3HT : IDT-2BR (1 : 0.6, w/w) active layers processed (a and c) without CN and (b and d) with 3% (v/v) CN.

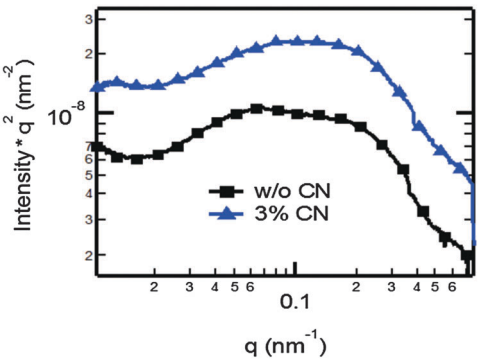

Fig. 8 R-SoXS profiles of P3HT : IDT-2BR (1 : 0.6, w/w) active layers processed without CN and with 3% (v/v) CN.

The phase separation of the blended film of P3HT:IDT-2BR is further investigated by resonant soft X-ray scattering (R-SoXS).[63,64] The optical contrast between different organic components can be significantly enhanced by using resonant energies near the carbon K-edge. The scattering profiles are displayed in Fig. 8. It is interesting to note that the phase separation is reasonably small with a median domain size of ~30–50 nm. The average composition variation (or relative domain purity) can be extracted from R-SoXS. The relative domain purity of 65% and 100% is obtained for blended films without CN and with 3% CN, respectively, suggesting that domains become much purer after processing with CN. The purer domains reduce bimolecular recombination and are thus favourable for device performance.[63–65]

In summary, an A–D–A type non-fullerene acceptor IDT-2BR was designed, calculated, synthesized and used in PSCs. IDT-2BR adopts a nearly flat backbone configuration, which facilitates charge transport, while the hexylphenyl groups on the IDT moiety exhibit a dihedral angle of *ca.* 115° to the backbone plane, which is beneficial for forming favourable interpenetrating networks without severe self-aggregation when mixing with P3HT. IDT-2BR exhibits excellent thermal stability, strong and broad absorption from 300 to 750 nm complemented with that of P3HT, appropriate LUMO and HOMO energy levels matched with those of P3HT, and relatively high electron mobility. Fullerene-free PSCs based on P3HT : IDT-2BR (1 : 0.6, w/w) blended films processed with 3% CN achieved PCEs as high as 5.12%, which is much higher than that of $PC_{61}BM$-based control devices (3.71%) and is the highest value reported for P3HT-based fullerene-free PSCs. Interestingly, the PCE values changed only 10% when varying the thickness of the active layer from 60 nm to 220 nm, which is beneficial to device reproducibility and scalable roll-to-roll fabrication. P3HT:IDT-2BR blended films processed with 3% CN exhibit clear interpenetrating networks, reasonably small phase separation, and pure domains, which facilitate exciton dissociation, charge transport and thus efficiency enhancement.

Experimental section

Synthesis of compound 3

To a three-necked round-bottomed flask were added compound **1** (494 mg, 0.40 mmol), compound **2** (243 mg, 1.0 mmol), and

toluene (30 mL). The mixture was deoxygenated with argon for 15 min, and then $Pd(PPh_3)_4$ (30 mg, 0.026 mmol) was added. The mixture was refluxed for 48 h and then cooled to room temperature. 5 mL of aqueous KF solution (0.1 g mL^{-1}) was added and stirred at room temperature overnight to remove the tin impurity. 100 mL of water was added and the mixture was extracted with CH_2Cl_2 (2 × 100 mL). The organic phase was dried over anhydrous $MgSO_4$. After removing the solvent, the residue was purified by column chromatography on silica gel using petroleum ether/CH_2Cl_2 (1 : 2) as an eluent yielding a violet solid (342 mg, 69.5%). ^{1}H-NMR (400 MHz, CD_2Cl_2): δ 10.70 (s, 2H), 8.27 (s, 2H), 8.19 (d, J = 7.6 Hz, 2H), 8.00 (d, J = 7.6 Hz, 2H), 7.65 (s, 2H), 7.28 (d, J = 8.4 Hz, 8H), 7.14 (d, J = 8.4 Hz, 8H), 2.60 (m, 8H), 1.58 (m, 8H), 1.29 (m, 24H), 0.86 (m, 12H). ^{13}C-NMR (100 MHz, $CDCl_3$): δ 188.2, 157.6, 154.5, 153.6, 151.9, 146.5, 142.1, 141.6, 136.0, 133.2, 132.6, 128.8, 128.1, 125.8, 125.0, 122.9, 118.5, 63.4, 35.7, 31.8, 31.5, 29.3, 22.7, 14.2. MS (MALDI): m/z 1231 (M^+). Anal. calc. for $C_{78}H_{78}N_4O_2S_4$: C, 76.06; H, 6.38; N, 4.55. Found: C, 75.91; H, 6.36; N, 4.60.

Synthesis of IDT-2BR

To a three-necked round-bottomed flask were added compound **3** (202 mg, 0.16 mmol), 3-ethylrhodanine (258 mg, 1.6 mmol), chloroform (30 mL), and triethylamine (1 mL). The mixture was deoxygenated with nitrogen for 15 min and then refluxed for 12 h. After cooling to room temperature, the mixture was poured into methanol (200 mL) and filtered. The residue was purified by column chromatography on silica gel using petroleum ether/CH_2Cl_2 (1 : 1) as an eluent yielding a dark blue solid (129 mg, 53.1%). ^{1}H-NMR (400 MHz, CD_2Cl_2): δ 8.42 (s, 2H), 8.22 (s, 2H), 7.95 (d, J = 7.6 Hz, 2H), 7.67 (d, J = 7.6 Hz, 2H), 7.63 (s, 2H), 7.28 (d, J = 8.4 Hz, 8H), 7.14 (d, J = 8.4 Hz, 8H), 4.23 (m, 4H), 2.59 (m, 8H), 1.58 (m, 8H), 1.29 (m, 30H), 0.86 (m, 12H). ^{13}C-NMR (100 MHz, $CDCl_3$): δ 192.9, 167.5, 157.5, 154.5 154.3 151.6, 145.5, 141.8, 141.4, 135.8, 131.1, 130.1, 128.5, 127.9, 127.1, 125.1, 124.8, 124.6, 124.0, 118.2, 63.2, 40.0, 35.6, 31.8, 31.6, 29.2, 22.7, 13.9, 12.1. MS (MALDI): m/z 1517 (M^+). Anal. calc. for $C_{88}H_{88}N_6O_2S_8$: C, 69.62; H, 5.84; N, 5.54. Found: C, 69.57; H, 5.91; N, 5.47. $\lambda_{max,s}$ = 636 nm (1.3 × 10^5 M^{-1} cm^{-1}).

Fabrication and characterization of photovoltaic cells

Polymer solar cells were fabricated with the structure, ITO/PEDOT:PSS/P3HT:IDT-2BR/Ca/Al. The patterned indium tin oxide (ITO) glass (sheet resistance = 15 Ω □$^{-1}$) was pre-cleaned in an ultrasonic bath of acetone and isopropanol, and treated in an ultraviolet-ozone chamber (Jelight Company, USA) for 23 min. A thin layer (35 nm) of poly(3,4-ethylenedioxythiophene):poly(styrene sulfonate) (PEDOT:PSS, Baytron PVP AI 4083, Germany) was spin-coated onto the ITO glass and baked at 150 °C for 20 min. The P3HT:IDT-2BR mixture (25 mg mL^{-1} in total) in *o*-DCB without or with CN was spin-coated on the PEDOT:PSS layer to form a photosensitive layer. The calcium layer (*ca.* 20 nm) and the aluminum layer (*ca.* 100 nm) were then evaporated onto the surface of the photosensitive layer under vacuum (*ca.* 10^{-5} Pa) to form the negative electrode. The active area of the device was 4 mm^2. The *J–V* curve was measured using a computer-controlled B2912A precision source/measure unit (Agilent Technologies). An XES-70S1 (SAN-EI Electric Co., Ltd) solar simulator (AAA grade, 70 × 70 mm^2 photobeam size) coupled with AM 1.5G solar spectrum filters was used as the light source, and the optical power at the sample was 100 mW cm^{-2}. A 2 × 2 cm^2 monocrystalline silicon reference cell (SRC-1000-TC-QZ) was purchased from VLSI Standards Inc. The IPCE spectrum was measured using a solar cell spectral response measurement system QE-R3011 (Enlitech Co., Ltd). In order to investigate the dependence of J_{SC} on the light intensity, the light intensity was modulated with four neutral density filters. The light intensity at each wavelength was calibrated using a standard single crystal Si photovoltaic cell. Hole-only or electron-only diodes were fabricated using the architectures ITO/PEDOT:PSS/sample layer/Au for holes and Al/sample layer/Al for electrons. The mobility was extracted by fitting the current density–voltage curves using the Mott–Gurney relationship (space charge limited current).

Acknowledgements

We thank the NSFC (91433114, 51261130582, 21504006, 21534003), the 973 Project (2011CB808401) and the President's Undergraduate Research Fellowship of Peking University for financial support. The X-ray data were acquired at beamlines 11.0.1.2[66] and 7.3.3[67] at the Advanced Light Source, which is supported by the Director, Office of Science, Office of Basic Energy Sciences of the U.S. Department of Energy under Contract No. DE-AC02-05CH11231.

Notes and references

1 Y.-J. Cheng, S.-H. Yang and C.-S. Hsu, *Chem. Rev.*, 2009, **109**, 5868.
2 Y. Li, *Acc. Chem. Res.*, 2012, **45**, 723.
3 G. Li, R. Zhu and Y. Yang, *Nat. Photonics*, 2012, **6**, 153.
4 Y. Chen, X. Wan and G. Long, *Acc. Chem. Res.*, 2013, **46**, 2645.
5 L. Ye, S. Zhang, L. Huo, M. Zhang and J. Hou, *Acc. Chem. Res.*, 2014, **47**, 1595.
6 J. E. Anthony, A. Facchetti, M. Heeney, S. R. Marder and X. Zhan, *Adv. Mater.*, 2010, **22**, 3876.
7 Y. Liu, J. Zhao, Z. Li, C. Mu, W. Ma, H. Hu, K. Jiang, H. Lin, H. Ade and H. Yan, *Nat. Commun.*, 2014, **5**, 5293.
8 S. E. Shaheen, C. J. Brabec, N. S. Sariciftci, F. Padinger, T. Fromherz and J. C. Hummelen, *Appl. Phys. Lett.*, 2001, **78**, 841.
9 C.-C. Chen, W.-H. Chang, K. Yoshimura, K. Ohya, J. You, J. Gao, Z. Hong and Y. Yang, *Adv. Mater.*, 2014, **26**, 5670.
10 H. Zhou, Y. Zhang, C.-K. Mai, S. D. Collins, G. C. Bazan, T.-Q. Nguyen and A. J. Heeger, *Adv. Mater.*, 2015, **27**, 1767.
11 Y. He and Y. Li, *Phys. Chem. Chem. Phys.*, 2011, **13**, 1970.
12 G. Yu, J. Gao, J. C. Hummelen, F. Wudl and A. J. Heeger, *Science*, 1995, **270**, 1789.
13 T. Liu and A. Troisi, *Adv. Mater.*, 2013, **25**, 1038.
14 A. Tournebize, P.-O. Bussière, A. Rivaton, J.-L. Gardette, H. Medlej, R. C. Hiorns, C. Dagron-Lartigau, F. C. Krebs and K. Norrman, *Chem. Mater.*, 2013, **25**, 4522.
15 P. Sonar, J. P. F. Lim and K. L. Chan, *Energy Environ. Sci.*, 2011, **4**, 1558.
16 Y. Lin, Y. Li and X. Zhan, *Chem. Soc. Rev.*, 2012, **41**, 4245.

17 J. E. Anthony, *Chem. Mater.*, 2011, **23**, 583.
18 A. Facchetti, *Mater. Today*, 2013, **16**, 123.
19 Y. Lin and X. Zhan, *Mater. Horiz.*, 2014, **1**, 470.
20 X. Zhan, A. Facchetti, S. Barlow, T. J. Marks, M. A. Ratner, M. R. Wasielewski and S. R. Marder, *Adv. Mater.*, 2011, **23**, 268.
21 X. Zhao and X. Zhan, *Chem. Soc. Rev.*, 2011, **40**, 3728.
22 X. Zhan, Z. Tan, B. Domercq, Z. An, X. Zhang, S. Barlow, Y. Li, D. Zhu, B. Kippelen and S. R. Marder, *J. Am. Chem. Soc.*, 2007, **129**, 7246.
23 X. Zhang, Z. Lu, L. Ye, C. Zhan, J. Hou, S. Zhang, B. Jiang, Y. Zhao, J. Huang, S. Zhang, Y. Liu, Q. Shi, Y. Liu and J. Yao, *Adv. Mater.*, 2013, **25**, 5791.
24 Y. Lin, Y. Wang, J. Wang, J. Hou, Y. Li, D. Zhu and X. Zhan, *Adv. Mater.*, 2014, **26**, 5137.
25 D. Mori, H. Benten, I. Okada, H. Ohkita and S. Ito, *Energy Environ. Sci.*, 2014, **7**, 2939.
26 Y. Zhou, T. Kurosawa, W. Ma, Y. Guo, L. Fang, K. Vandewal, Y. Diao, C. Wang, Q. Yan, J. Reinspach, J. Mei, A. L. Appleton, G. I. Koleilat, Y. Gao, S. C. Mannsfeld, A. Salleo, H. Ade, D. Zhao and Z. Bao, *Adv. Mater.*, 2014, **26**, 3767.
27 Y. Zang, C.-Z. Li, C.-C. Chueh, S. T. Williams, W. Jiang, Z.-H. Wang, J.-S. Yu and A. K.-Y. Jen, *Adv. Mater.*, 2014, **26**, 5708.
28 J. Zhao, Y. Li, H. Lin, Y. Liu, K. Jiang, C. Mu, T. Ma, J. Y. Lin Lai, H. Hu, D. Yu and H. Yan, *Energy Environ. Sci.*, 2015, **8**, 520.
29 H. Li, T. Earmme, G. Ren, A. Saeki, S. Yoshikawa, N. M. Murari, S. Subramaniyan, M. J. Crane, S. Seki and S. A. Jenekhe, *J. Am. Chem. Soc.*, 2014, **136**, 14589.
30 Y. Liu, C. Mu, K. Jiang, J. Zhao, Y. Li, L. Zhang, Z. Li, J. Y. Lai, H. Hu, T. Ma, R. Hu, D. Yu, X. Huang, B. Z. Tang and H. Yan, *Adv. Mater.*, 2015, **27**, 1015.
31 O. K. Kwon, J.-H. Park, D. W. Kim, S. K. Park and S. Y. Park, *Adv. Mater.*, 2015, **27**, 1951.
32 C. Lee, H. Kang, W. Lee, T. Kim, K. H. Kim, H. Y. Woo, C. Wang and B. J. Kim, *Adv. Mater.*, 2015, **27**, 2466.
33 Y. J. Hwang, T. Earmme, B. A. Courtright, F. N. Eberle and S. A. Jenekhe, *J. Am. Chem. Soc.*, 2015, **137**, 4424.
34 X. Zhang, C. L. Zhan and J. N. Yao, *Chem. Mater.*, 2015, **27**, 166.
35 Y. Zhong, M. T. Trinh, R. Chen, W. Wang, P. P. Khlyabich, B. Kumar, Q. Xu, C.-Y. Nam, M. Y. Sfeir, C. Black, M. L. Steigerwald, Y.-L. Loo, S. Xiao, F. Ng, X.-Y. Zhu and C. Nuckolls, *J. Am. Chem. Soc.*, 2015, **136**, 15215.
36 W. Li, W. S. Roelofs, M. Turbiez, M. M. Wienk and R. A. Janssen, *Adv. Mater.*, 2014, **26**, 3304.
37 Y. Lin, J. Wang, Z. G. Zhang, H. Bai, Y. Li, D. Zhu and X. Zhan, *Adv. Mater.*, 2015, **27**, 1170.
38 Y. Lin, Z.-G. Zhang, H. Bai, J. Wang, Y. Yao, Y. Li, D. Zhu and X. Zhan, *Energy Environ. Sci.*, 2015, **8**, 610.
39 H. Bai, Y. Wang, P. Cheng, J. Wang, Y. Wu, J. Hou and X. Zhan, *J. Mater. Chem. A*, 2015, **3**, 1910.
40 J. W. Jung, J. W. Jo, C. C. Chueh, F. Liu, W. H. Jo, T. P. Russell and A. K. Jen, *Adv. Mater.*, 2015, **27**, 3310.
41 H. Li, Y. J. Hwang, B. A. Courtright, F. N. Eberle, S. Subramaniyan and S. A. Jenekhe, *Adv. Mater.*, 2015, **27**, 3266.
42 P. Cheng, L. Ye, X. Zhao, J. Hou, Y. Li and X. Zhan, *Energy Environ. Sci.*, 2014, **7**, 1351.
43 H. Bai, P. Cheng, Y. Wang, L. Ma, Y. Li, D. Zhu and X. Zhan, *J. Mater. Chem. A*, 2014, **2**, 778.
44 Y. Lin, J. Wang, S. Dai, Y. Li, D. Zhu and X. Zhan, *Adv. Energy Mater.*, 2014, **4**, 1400420.
45 H. Bai, Y. Wang, P. Cheng, Y. Li, D. Zhu and X. Zhan, *ACS Appl. Mater. Interfaces*, 2014, **6**, 8426.
46 Y. Li, K. Yao, H.-L. Yip, F.-Z. Ding, Y.-X. Xu, X. Li, Y. Chen and A. K.-Y. Jen, *Adv. Funct. Mater.*, 2014, **24**, 3631.
47 M. Manceau, E. Bundgaard, J. E. Carlé, O. Hagemann, M. Helgesen, R. Søndergaard, M. Jørgensen and F. C. Krebs, *J. Mater. Chem.*, 2011, **21**, 4132.
48 R. Søndergaard, M. Manceau, M. Jørgensen and F. C. Krebs, *Adv. Energy Mater.*, 2012, **2**, 415.
49 Y. Lin, P. Cheng, Y. Li and X. Zhan, *Chem. Commun.*, 2012, **48**, 4773.
50 Y. Lin, Y. Li and X. Zhan, *Adv. Energy Mater.*, 2013, **3**, 724.
51 K. N. Winzenberg, P. Kemppinen, F. H. Scholes, G. E. Collis, Y. Shu, T. Birendra Singh, A. Bilic, C. M. Forsyth and S. E. Watkins, *Chem. Commun.*, 2013, **49**, 6307.
52 Q. Yan, Y. Zhou, Y.-Q. Zheng, J. Pei and D. Zhao, *Chem. Sci.*, 2013, **4**, 4389.
53 Y. Zhou, Y.-Z. Dai, Y.-Q. Zheng, X.-Y. Wang, J.-Y. Wang and J. Pei, *Chem. Commun.*, 2013, **49**, 5802.
54 J. T. Bloking, T. Giovenzana, A. T. Higgs, A. J. Ponec, E. T. Hoke, K. Vandewal, S. W. Ko, Z. N. Bao, A. Sellinger and M. D. McGehee, *Adv. Energy Mater.*, 2014, **4**, 1301426.
55 Y. Kim, C. E. Song, S.-J. Moon and E. Lim, *Chem. Commun.*, 2014, **50**, 8235.
56 Y. Yang, G. Zhang, C. Yu, C. He, J. Wang, X. Chen, J. Yao, Z. Liu and D. Zhang, *Chem. Commun.*, 2014, **50**, 9939.
57 S. Holliday, R. S. Ashraf, C. B. Nielsen, M. Kirkus, J. A. Rohr, C. H. Tan, E. Collado-Fregoso, A. C. Knall, J. R. Durrant, J. Nelson and I. McCulloch, *J. Am. Chem. Soc.*, 2015, **137**, 898.
58 O. K. Kwon, J.-H. Park, S. K. Park and S. Y. Park, *Adv. Energy Mater.*, 2015, **5**, 1400929.
59 Z. Mao, W. Senevirathna, J.-Y. Liao, J. Gu, S. V. Kesava, C. Guo, E. D. Gomez and G. Sauvé, *Adv. Mater.*, 2014, **26**, 6290.
60 W. Senevirathna, J.-y. Liao, Z. Mao, J. Gu, M. Porter, C. Wang, R. Fernando and G. Sauve, *J. Mater. Chem. A*, 2015, **3**, 4203.
61 S. R. Cowan, A. Roy and A. J. Heeger, *Phys. Rev. B: Condens. Matter Mater. Phys.*, 2010, **82**, 245207.
62 A. K. Kyaw, D. H. Wang, D. Wynands, J. Zhang, T. Q. Nguyen, G. C. Bazan and A. J. Heeger, *Nano Lett.*, 2013, **13**, 3796.
63 H. Yan, B. A. Collins, E. Gann, C. Wang, H. Ade and C. R. McNeill, *ACS Nano*, 2012, **6**, 677.
64 W. Ma, J. R. Tumbleston, M. Wang, E. Gann, F. Huang and H. Ade, *Adv. Energy Mater.*, 2013, **3**, 864.
65 W. Ma, J. R. Tumbleston, L. Ye, C. Wang, J. Hou and H. Ade, *Adv. Mater.*, 2014, **26**, 4234.
66 E. Gann, A. T. Young, B. A. Collins, H. Yan, J. Nasiatka, H. A. Padmore, H. Ade, A. Hexemer and C. Wang, *Rev. Sci. Instrum.*, 2012, **83**, 045110.
67 A. Hexemer, W. Bras, J. Glossinger, E. Schaible, E. Gann, R. Kirian, A. MacDowell, M. Church, B. Rude and H. Padmore, *J. Phys.: Conf. Ser.*, 2010, **247**, 012007.